Characterization of fluorescent proteins, promoters, and selectable markers for applications in the Lyme disease spirochete *Borrelia burgdorferi*.

Running title: Molecular tools for the Lyme disease agent

Constantin N. Takacs[1,2,3], Zachary A. Kloos[1,4], Molly Scott[1,2,3], Patricia A. Rosa[5], and Christine Jacobs-Wagner[1,2,3,6,*]

[1] Microbial Sciences Institute, Yale West Campus, West Haven, CT, 06516, USA.

[2] Department of Molecular, Cellular, and Developmental Biology, Yale University, New Haven, CT, 06511, USA.

[3] Howard Hughes Medical Institute, Yale West Campus, West Haven, CT, 06516, USA.

[4] Microbiology Program, Yale University, New Haven, CT, 06511, USA.

[5] Laboratory of Bacteriology, Rocky Mountain Laboratories, Division of Intramural Research, National Institute of Allergy and Infectious Diseases, National Institutes of Health, Hamilton, MT, 59840, USA

[6] Department of Microbial Pathogenesis, Yale School of Medicine, New Haven, CT, 06536, USA

* To whom correspondence should be addressed. Tel: +1 203 737-6778; Fax: +1 203 737-6715; Email: christine.jacobs-wagner@yale.edu.

ABSTRACT

Lyme disease is the most widely reported vector-borne disease in the United States. Its incidence is rapidly increasing and disease symptoms can be debilitating. The need to understand the biology of the disease agent, the spirochete *Borrelia burgdorferi*, is thus evermore pressing. Despite important advances in *B. burgdorferi* genetics, the array of molecular tools available for use in this organism remains limited, especially for cell biological studies. Here, we adapt a palette of bright and mostly monomeric fluorescent proteins for versatile use and multi-color imaging in *B. burgdorferi*. We also characterize two novel antibiotic selection markers and establish the feasibility of their use in conjunction with extant markers. Lastly, we describe a set of constitutively active promoters of low and intermediate strengths that allow fine-tuning of gene expression levels. These molecular tools complement and expand current experimental capabilities in *B. burgdorferi,* which will facilitate future investigation of this important human pathogen. To showcase the usefulness of these reagents, we used them to investigate the subcellular localization of BB0323, a *B. burgdorferi* lipoprotein essential for survival in the host and vector environments. We show that BB0323 accumulates at the cell poles and future division sites of *B. burgdorferi* cells, highlighting the complex subcellular organization of this spirochete.

IMPORTANCE

Genetic manipulation of the Lyme disease spirochete *B. burgdorferi* remains cumbersome, despite significant progress in the field. The scarcity of molecular reagents available for use in this pathogen has slowed research efforts to study its unusual biology. Of interest, *B. burgdorferi* displays complex cellular organization features that have yet to be understood. These include an unusual morphology and a highly fragmented genome, both of which are likely to play important roles in the bacterium's transmission, infectivity, and persistence. Here,

we complement and expand the array of molecular tools available for use in *B. burgdorferi* by generating and characterizing multiple fluorescent proteins, antibiotic selection markers, and constitutively active promoters of different strengths. These tools will facilitate investigations in this important human pathogen, as exemplified by the polar and midcell localization of the cell envelope regulator BB0323, which we uncovered using these reagents.

INTRODUCTION

Lyme disease, a widespread infection transmitted by hard ticks of the *Ixodes* genus, is the most prevalent vector-borne disease in the United States. The disease is also common in Europe and Asia, and its incidence and geographic distribution have been steadily increasing in recent decades (1). Lyme disease is caused by spirochetal bacteria belonging to the *Borrelia burgdorferi* sensu lato group, with *B. burgdorferi* sensu stricto (hereafter referred to as *B. burgdorferi*) being the principal agent in North America, and *B. afzelii* and *B. garinii* being the primary agents in Eurasia. In humans, acute Lyme disease is often associated with a characteristic skin rash and flu-like symptoms. If left untreated, late stages of infection may result in carditis, neurological manifestations, and arthritis (2).

Spirochetes in general, and the *Borrelia* species in particular, display cellular features unusual for bacteria (3). Spirochete cells are typically very long and thin by bacterial standards. *B. burgdorferi* cells, for example, are 10 to 25 µm long and ~250 nm wide (4-6). Spirochetes are also highly motile, but, unlike most bacteria, their flagella are not external organelles (7). Instead, these flagella are located in the periplasm (i.e., between the inner and outer membranes). In *B. burgdorferi,* the helicity of the flagella imparts the flat-wave morphology of the bacterium (8). *B. burgdorferi* also possesses what is likely the most segmented genome of any bacterium investigated to date. It is made up of a linear chromosome of about 900 kilobases (kb) and over 20 linear and circular genetic elements ranging from 5 to 60 kb in length (9, 10). These smaller genetic elements are often referred to as plasmids, though many of them encode proteins that are essential for the life cycle of this organism (11). Recent work from our laboratory has shown that *Borreliae* species also have an uncommon pattern of cell wall synthesis in which discrete zones of cell elongation in one generation predetermine the division sites of daughter cells in the next generation (6).

While these unusual cellular features are integral to *B. burgdorferi* physiology and pathogenesis, little is known about how they arise or are maintained over generations. In fact, the cell biology of this pathogen remains largely unexplored. Technical hurdles have slowed progress in this area. Genetic manipulation of *B. burgdorferi* is feasible, but the available genetic tools are still limited, and the process remains cumbersome (12, 13). Constitutive gene expression is mostly limited to the use of very strong promoters. Moreover, apart from a few exceptions (14-19), fluorescent protein reporters have primarily been used as gene expression reporters or as cellular stains for *in vivo* localization of the spirochete (13). Yet fluorescent proteins have many more uses, which have transformed the field of cell biology (20). For example, fluorescent proteins have opened the door to localization studies in live cells. They have also facilitated the detection of protein-protein interactions, the measurement of physical properties of cells, and the investigation of single events and of population heterogeneity. Much of this information is not accessible through the use of bulk biochemical measurements on cell populations. The averaging inherent to such techniques leads to loss of spatial resolution and obscures rare events and cell-to-cell or subcellular heterogeneity of behaviour (21). Indeed, the ability to perform extensive genetic manipulations and to use a wide panel of fluorescent proteins in an organism has been key to progress in understanding bacterial cell biology (22). Such approaches have been used extensively in model bacteria such as *Bacillus subtilis*, *Escherichia coli*, and *Caulobacter crescentus* since the first reported use of fluorescent protein fusions two decades ago (23-25). In order to facilitate the study of *B. burgdorferi*, we have generated new investigative tools by characterizing a panel of fluorescent proteins, promoters and antibiotic resistance markers for use in this medically important bacterium. We exemplify the usefulness of these reagents by creating an mCherry fusion to BB0323, a multifunctional *B. burgdorferi* lipoprotein required for outer membrane stability (26-28) and essential for the spirochete's survival in the tick vector and the mammalian host (27). Using

this fusion, we show that BB0323 localizes at the spirochete's poles and at future division sites, highlighting underappreciated spatial and temporal organization principles of *B. burgdorferi* cells. (An earlier version of this article was submitted to the online preprint archive BioRxiv [doi: https://doi.org/10.1101/363390])

MATERIALS AND METHODS

Bacteria, growth conditions, and genetic transformations

Bacterial strains used in this study are listed in Table 1. *E. coli* strains were grown at 30 °C in liquid culture in Super Broth medium (35 g/L bacto-tryptone, 20 g/L yeast extract, 5 g/L NaCl, 6 mM NaOH) with shaking, or on LB agar plates. Plasmids were transformed by electroporation or heat shock. For selection of *E. coli* strains we used 200 µg/mL (solid medium) or 100 µg/mL (liquid medium) ampicillin, 20 µg/mL (solid medium) or 15 µg/mL (liquid medium) gentamicin, 50 µg/mL kanamycin (solid and liquid media), 50 µg/mL spectinomycin (solid medium), 50 µg/mL streptomycin (liquid medium), and 25 µg/mL (liquid medium) or 50 µg/mL (solid medium) rifampicin.

B. burgdorferi strains were grown in BSK-II medium supplemented with 6% (v/v) heat inactivated rabbit serum (Sigma Aldrich or Gibco) or in complete BSK-H medium (Sigma Aldrich), as previously described (29-31). Cultures were incubated at 34 °C under 5% CO_2 atmosphere in a humidified incubator. Antibiotics were used at the following concentrations (unless otherwise indicated): gentamicin at 40 µg/mL, streptomycin at 100 µg/mL, kanamycin at 200 µg/mL, blasticidin S at 10 µg/mL, and hygromycin B at 250 µg/mL. Ampicillin was purchased from Fisher Scientific, blasticidin S and hygromycin B from Invivogen, and all other antibiotics and biliverdin hydrochloride from Sigma Aldrich.

B. burgdorferi strain generation

B. burgdorferi electrocompetent cells were prepared as previously described (32) and were transformed with shuttle vector plasmid DNA (usually 30 µg) by electroporation. Electroporated cells were then allowed to recover overnight in BSK-II medium at 34 °C. The next day, the transformants were plated in semi-solid BSK-agarose medium with appropriate antibiotics as previously described (32). Individual colonies were then expanded and characterized. Alternatively, antibiotic selection was initiated in liquid medium and 5-fold serial dilutions of the culture were plated in a 96-well plate (24 wells for each dilution). After 10-14 days of incubation, the wells were inspected by microscopy using dark-field illumination. Based on Poisson distribution probability, when fewer than 20% of the wells of a given dilution were positive for growth, those wells were considered to contain clonal populations and were further expanded and characterized as such. When appropriate, fluorescence imaging was used to confirm fluorescent protein expression. Alternatively, selected, non-clonal transformant populations were enumerated using C-Chip disposable hemocytometers (INCYTO), using the manufacturer's instructions with the following change: counting was done by continuously scanning the full height of the counting chamber for each counting surface to account for the height of the counting chamber being larger than the size of the spirochetes. Enumerated spirochetes were then diluted in BSK-II medium and plated in 96-well plates at an average density of 0.2 cells/well. After 10-14 days, clonal growth was confirmed by dark-field microscopy imaging.

Determination of minimal inhibitory concentrations (MIC) and antibiotic cross-resistance

MICs were determined using strains B31 e2 or B31 MI, while cross-resistance testing was done using B31 e2-derived strains that contained shuttle vectors carrying kanamycin,

gentamicin, streptomycin, blasticidin S, or hygromycin B resistance markers (see strains CJW_Bb069 through CJW_Bb073 in Table 1). For both tests, antibiotics were two-fold serially diluted in complete BSK-II or BSK-H medium. For each concentration, 100 µL of antibiotic solution were dispensed into two to four wells of 96-well plates. The cell density of *B. burgdorferi* cultures was determined by direct counting using dark-field microscopy. The cultures were then diluted to 2×10^4 cells/mL in antibiotic-free medium, and 100 µL of this diluted culture were added to the antibiotic-containing wells to yield an inoculum of 10^4 cells/mL. The plates were incubated for at least 4 days at 34 °C under 5% CO_2 atmosphere in a humidified incubator, after which each well was checked for spirochete growth and motility using dark-field microscopy. A well was marked as positive if motile cells were detected. The plates were further incubated for several days, during which bacterial growth-dependent acidification caused the phenol red pH indicator in the medium to change color. This color change was documented using colorimetric trans-illumination imaging on a GE Amersham Imager 600. We verified that growth scoring of each well by dark-field imaging matched the observed medium color change.

DNA manipulations

Plasmids used in this study are listed in Table 2. Methods of plasmid construction and sequences of oligonucleotide primers are provided as Supplemental Material. Standard molecular biology techniques were used, as detailed in the Supplemental Material. Codon optimization was performed using the web-based Java Codon Adaptation Tool hosted at www.jcat.de (33) and the codon usage table for *B. burgdorferi* as stored at www.kazusa.or.jp/codon (34). Codon-optimized DNA sequences were then chemically synthesized at Genewiz. DNA sequences of each codon-optimized gene are provided in the Supplemental Material. They are also available at GenBank under the accession numbers

MH644044 through MH644053. The names of these genes include a *Bb* superscript to indicate that the gene's nucleotide sequence is codon-optimized for translation in *B. burgdorferi* (e.g., *iRFP*^{Bb}). The name of the protein encoded by such a gene (e.g., iRFP), however, does not include the Bb superscript, as the protein's amino acid sequence does not differ from that expressed from other versions of the gene.

Microscopy

Visualization and counting of live spirochetes were done using a Nikon Eclipse E600 microscope equipped with dark-field illumination optics and a Nikon 40X 0.55 numerical aperture (NA) phase contrast air objective. Phase contrast and fluorescence imaging was done on a Nikon Eclipse Ti microscope equipped with a 100X Plan Apo 1.40 NA phase contrast oil objective, a Hamamatsu Orca-Flash4.0 V2 Digital CMOS camera, a Sola light engine (Lumencor), and controlled by the Metamorph software (Molecular Devices). Alternatively, light microscopy was performed on a Nikon Ti microscope equipped with a 100X Plan Apo 1.45 NA phase contrast oil objective, a Hamamatsu Orca-Flash4.0 V2 CMOS camera, a Spectra X light engine (Lumencor) and controlled by the Nikon Elements software. Excitation of iRFP was achieved using the 640/30 nm band of the SpectraX system, but higher excitation efficiency and thus brightness could in theory be obtained using a red-shifted excitation source between 660 and 680 nm. The following Chroma filter sets were used to acquire fluorescence images: CFP (excitation ET436/20x, dichroic T455lp, emission ET480/40m), GFP (excitation ET470/40x, dichroic T495lpxr, emission ET525/50m), YFP (excitation ET500/20x, dichroic T515lp, emission ET535/30m), mCherry/TexasRed (excitation ET560/40x, dichroic T585lpxr, emission ET630/75m), and Cy5.5 (excitation ET650/45x, dichroic T685lpxr, emission ET720/60m). For imaging, cultures were inoculated at densities between 10^3 and 10^5 cells/mL, and grown for two to three days to reach densities between 10^6 and 3×10^7 cells/mL. The cells

were then immobilized on a 2% agarose pad (6, 35) made with phosphate buffered saline covered with a No. 1.5 coverslip, after which the cells were immediately imaged live. Images were processed using the Metamorph software. Figures were generated using Adobe Illustrator software.

Image analysis

Cell outlines were generated using phase contrast images and the open-source image analysis software Oufti (36). Outlines were checked visually for each cell and were extended manually to the full length of the cells when appropriate. When not assigned to single cells or assigned to non-cellular debris, outlines were manually removed. The remaining outlines were further refined using the Refine All function of the software. To quantify fluorescence signals, individual cytoplasmic cylinders connected by an outer membrane bridge (i.e., late predivisional cells with two separated cytoplasms) were treated as independent cellular units. For demograph analysis of strain CJW_Bb173, late predivisional cells were considered to form one cell. Fluorescence signal data was added to the cells and demographs were generated in Oufti. The resulting cell lists were processed using the MATLAB script addMeshtoCellList.m (see Supplemental Material for the code). This script uses the functions CL_getframe.m, CL_removeCell.m, CL_cellId2PositionInFrame.m, and getextradata.m, which were previously described (36). Single-cell fluorescence intensity values were calculated by dividing the total fluorescence signal inside a cell outline by the cell's area using the MATLAB-based function CalculateFluorPerCell.m. Final fluorescence data were plotted using the GraphPad Prism 5 software. The number of cells analyzed for each condition is provided in the Supplemental Material.

RESULTS

A wide palette of fluorescent proteins for imaging in *B. burgdorferi*

Only a few fluorescent proteins have been used to date in *B. burgdorferi* (summarized in Table 3). These proteins belong primarily to two color classes: green fluorescent proteins (GFP) and red fluorescent proteins (RFP) (Table 3). To expand the range of options for multi-color imaging of *B. burgdorferi*, we focused on a set of fluorescent proteins that have been used in localization studies in other organisms and codon-optimized their genes for translation in *B. burgdorferi*. The selected proteins span five color classes (Table 3) and their signal can be collected using widely available filter sets for cyan fluorescent protein (CFP), GFP, yellow fluorescent protein (YFP), mCherry/TexasRed and Cy5.5 fluorescence. The selected cyan, green, and yellow variants are all derivatives of the jellyfish (*Aequorea victoria*) GFP. We used both the classic variants Cerulean (37), enhanced GFP, or EGFP (38), Citrine (39), as well as the superfolder (e.g., sfGFP) variants (40). All variants included the monomeric mutation A206K (41), denoted by a lower case m before the name of the protein (e.g., mCerulean). Our red protein of choice was mCherry (42), a monomeric, improved variant of mRFP1. Lastly, we codon-optimized and expressed an infrared fluorescent protein, iRFP (43). The far-red wavelengths used to excite this fluorophore are less toxic to cells than the shorter excitation wavelengths used for the other fluorescent proteins, and the sample autofluorescence in the near-infrared spectral region is lower than in the other, blue-shifted imaging windows (20, 44).

To visualize these fluorescent proteins, we expressed them in strain B31 e2 from the strong flagellin promoter P_{flaB} (45) located on a shuttle vector. With the exception of iRFP, each fluorescent protein displayed bright fluorescence when imaged using a filter set matched to its color (Figure 1A). Unlike the other fluorescent proteins, which oxidatively conjugate their own amino acid side chains to create a fluorophore (20), iRFP covalently binds an exogenous biliverdin molecule, which then serves as the fluorophore (43). Adding the biliverdin cofactor to

the growth medium of the iRFP-expressing strain rendered the cells fluorescent in the near-infrared region of the spectrum, as detected with a Cy5.5 filter set (Figure 1B). Treating a control strain carrying an empty shuttle vector with biliverdin did not cause any increase in cellular fluorescence (data not shown). To measure cellular fluorescence levels, we chose a microscopy-based approach in conjunction with quantitative image analysis. This allowed us to efficiently analyze hundreds of cells and to clearly distinguish individual cells from similarly-sized debris found in the culture medium, or from clumps of multiple cells. Using this method, we established that a 4 μM concentration of biliverdin in the growth medium was sufficient to achieve maximal cellular brightness (Figure 1C). Close-to-maximal iRFP brightness was reached as early as an hour after addition of biliverdin to the culture and was maintained throughout subsequent growth (Figure 1D). Furthermore, continuous growth of *B. burgdorferi* in the presence of biliverdin was indistinguishable from growth in biliverdin-free medium (Figure 1E). This indicates that culture experiments that involve iRFP may be performed either by adding biliverdin shortly before imaging or by growing the cells continuously in the presence of biliverdin.

In microscopy studies, simultaneous imaging of multiple fluorescent proteins requires that the signal generated by a given fluorescent protein does not overlap with the fluorescence channels used to collect the signal of another protein. To assess the viability of using our palette of fluorescent proteins for multi-color imaging in *B. burgdorferi*, we quantified the signal generated by each fluorescent protein when imaged with the commonly used CFP, GFP, YFP, mCherry, and Cy5.5 filter cubes (Figure 2). We found that each fluorescent protein generated a strong signal when imaged with a color-matched filter set (Figure 2). As expected, we detected a significant spectral overlap between CFP and GFP, as well as between GFP and YFP variants. Importantly, signal quantification showed that mCerulean or msfCFP can be imaged alongside mCitrine, mCherry, and iRFP, while mEGFP or msfGFP can be imaged

alongside mCherry and iRFP, opening the door to combinatorial imaging of up to four proteins in the same *B. burgdorferi* cell.

Promoters for various levels of constitutive expression in *B. burgdorferi.*

To date, constitutive expression of exogenous genes in *B. burgdorferi*, including antibiotic selection markers and reporter genes such as fluorescent proteins and luciferases, has almost exclusively relied on very strong promoters such as P_{flaB} and P_{flgB} (13, 45). Reporter expression from strong promoters facilitates spirochete detection, particularly in high fluorescence background environments such as the tick midgut or mammalian tissues (46-48). However, as overexpression can affect protein localization, interfere with function, or cause cellular toxicity (e.g., (49-59)), lower levels of gene expression have proven instrumental in facilitating localization studies (e.g., (60-63)) and are often preferred in such applications.

To identify constitutively expressed promoters of low and medium strengths, we mined a published RNA sequencing (RNA-seq) dataset that measured transcript levels in cultures of *B. burgdorferi* in early-exponential, mid-exponential and stationary phases of growth (64). We selected five genes whose expression was largely unchanged among the three growth phases tested (Figure 3A), amplified a DNA region upstream of each gene's predicted translational start site, and fused it to an mCherry reporter in a kanamycin resistance-conferring shuttle vector (Figure 3B). The amplified putative promoter sequences ranged in size from 129 to 212 base pairs (bp) and included the reported 5' untranslated regions (5'UTRs) of the downstream genes (64, 65). We also included in our analysis an empty vector and a vector containing a P_{flaB}-*mCherry*^{Bb} fusion, which served as references for no and high expression, respectively.

We transformed these constructs into *B. burgdorferi*, imaged the resulting strains, and quantified the fluorescence level in each cell. All promoters elicited fluorescence levels above the background of the strain carrying the empty vector (Figure 3C). We noticed differences

between the RNA-seq and mCherry reporter-based methods of measuring promoter strength, as detailed in the discussion. Importantly, however, the promoters we tested displayed a broad dynamic range from low (P_{0526}) to intermediate (P_{0826}, P_{resT}, P_{0031}, and P_{0026}) to high (P_{flaB}) strength.

Antibiotic selection in *B. burgdorferi* using hygromycin B and blasticidin S resistance markers

Several antibiotic resistance markers have been used to perform genetic manipulations in *B. burgdorferi* and have recently been reviewed in detail (13). The most widely used today are the kanamycin (*aphI*), gentamicin (*aacC1*), streptomycin (*aadA*) and erythromycin (*ermC*) resistance genes (see Table 4) (45, 66-68). Use of several other antibiotics for selection is either ineffective (e.g., zeocin, chloramphenicol, and puromycin), discouraged due to safety concerns (e.g., tetracyclines, β-lactams, and sometimes erythromycin), redundant due to cross-resistance (several aminoglycoside antibiotics), or no longer widespread (coumermycin A_1) due to alterations in cell physiology induced by both the antibiotic and the resistance marker (13, 67).

To expand the panel of antibiotic resistance markers that can be used in *B. burgdorferi*, we focused on two antibiotics commonly used for selection of eukaryotic cells, namely the translation inhibitors hygromycin B and blasticidin S. Rendering *B. burgdorferi* resistant to them does not pose a biosafety concern, as these antibiotics are not used to treat Lyme disease. We found that hygromycin B and blasticidin S prevented *B. burgdorferi* growth in liquid culture at concentrations of 200 and 5 µg/mL, respectively (Table 4). For resistance cassettes, we used the *E. coli* gene *hph* (also known as *aph(4)-Ia*), which encodes a hygromycin B phosphotransferase, and the *Aspergillus terreus* gene *bsd*, which encodes a blasticidin S deaminase (69-71). We codon-optimized these genes for translation in *B. burgdorferi* and

placed them under the control of the strong P_{flgB} promoter on a shuttle vector (Figure 4A). The resulting vectors, pBSV2H and pBSV2B, also carry the rifampicin resistance gene *arr-2* of *Pseudomonas aeruginosa* (72-74), which encodes a rifampicin ADP-ribosyltransferase. *B. burgdorferi* is naturally resistant to rifampicin (75, 76), but the use of rifampicin for selection in *E. coli* instead of the more expensive blasticidin S and hygromycin B antibiotics reduces the cost of generating and propagating the vectors in *E. coli*.

B. burgdorferi strains obtained by transforming pBSV2B or pBSV2H into B31 e2 grew readily in cultures containing 10 µg/mL blasticidin S or 250 µg/mL hygromycin B, respectively. We used these strains to test whether the antibiotic resistance cassettes encoded by these vectors conferred any cross-resistance to the often-used antibiotics kanamycin, gentamicin, streptomycin, and erythromycin. In parallel, we performed reciprocal tests using B31 e2-derived strains that carried a kanamycin, gentamicin, or streptomycin resistance cassette. Each strain was grown in the presence of two-fold serial dilutions of each antibiotic (Figure 4B). Each dilution series was centred on the concentration routinely used for selection with each of the tested antibiotics (Figure 4B, arrow). We incubated all cultures for at least four days and then inspected each well for growth by dark-field imaging. A well was considered to be growth-positive if we detected at least one motile spirochete after scanning a minimum of five fields of view. In addition, we further incubated the plates to allow for growth-dependent acidification of the medium. This pH change is easily detected as a change in the color of the medium from red, denoting no growth, to orange or yellow, denoting various degrees of growth (Figure 4C-H) (67). We confirmed that wells with the lowest antibiotic concentration at which the medium remained red also did not contain motile spirochetes. This concentration was taken to represent the minimum inhibitory concentration, or MIC (Figure 4C, black line). Whenever we exposed a strain to the antibiotic to which it carried a resistance gene, we readily detected growth at all antibiotic concentrations tested (Figure 4D-H), highlighting the efficacy of each

resistance marker. Importantly, we did not detect any major cross-resistance between the five resistance markers and the six antibiotics tested (Figure 4D-H). One exception was the kanamycin-resistant strain CJW_Bb069, which was able to grow in the presence of as much as 40 µg/mL gentamicin (Figure 4E), a concentration routinely used for gentamicin selection (67). A slightly higher amount of gentamicin (80 µg/mL) was, however, sufficient to kill this kanamycin-resistant strain (Figure 4E). This low level of cross-resistance may thus necessitate use of a higher dose of gentamicin for selection if the parental strain is already kanamycin-resistant.

Subcellular localization of a *B. burgdorferi* LysM domain-containing protein.

To highlight the usefulness of our newly generated *B. burgdorferi* molecular reagents, we fused the gene encoding mCherry to the 3' end of *bb0323* to create a C-terminal fluorescent fusion. The resulting construct was placed under the control of the intermediate-strength promoter P_{0826}. BB0323 is an important lipoprotein that is required for *B. burgdorferi*'s natural infection cycle through the tick and the mammalian reservoir (27). This lipoprotein is proteolytically processed into an N-terminal domain mediating outer membrane stability and cell separation, and a C-terminal fragment containing a peptidoglycan-binding LysM domain (26, 28, 77). The N- and C-terminal fragments interact with each other and were proposed to help anchor the outer membrane to the peptidoglycan (28).

We found that the BB0323-mCherry fusion displays striking localization patterns that vary predictably with the culture growth phase (Figure 5). In an exponentially growing culture, the shortest cells (likely newly born cells) displayed a patchy distribution of the BB0323-mCherry signal along the length of the cell, accompanied by accumulation of this signal at the cell poles (Figure 5A.i and 5B.i). In longer cells (i.e., later during the cell cycle), these patchy and bipolar localizations were accompanied by accumulation of the signal at midcell (Figure 5A.ii and 5B.ii).

These midcell localization events coincided with future division sites (6), though signal accumulation at midcell could be detected in the absence of obvious cell constriction (Figure 5.A.ii and 5B.ii). Midcell localization persisted through cell constriction, with the fluorescent signal often becoming split into two intensity peaks that flanked the cell constriction site, as shown by the indentation in the phase contrast signal (Figure 5A.iii and 5B.iii). Upon complete cell separation, these pairs of midcell intensity peaks presumably form the polar signals of daughter cells. In a subset of deeply constricted cells, BB0323-mCherry also accumulated at the 1/4 and 3/4 locations along the cell length (Figure 5A.iv and 5B.iv), which represent the midcell positions and future division sites of the still-connected daughter cells.

The cell cycle coordination of these localization patterns was confirmed by demograph analysis of static images of an asynchronous population (Figure 5C). In this representation, each horizontal line represents the distribution of the BB0323-mCherry fluorescent signal along the length of a single cell, as depicted in a heat map. Cells are sorted by their lengths to approximate cell cycle progression.

In a stationary phase culture, the same localization patterns were observed, except for the disappearance of the signal at the 1/4 and 3/4 cell positions. We assume that the slower growth rates in stationary phase ensure that daughter cells fully separate before BB0323-mCherry begins to accumulate at midcell. Slower growth rates in stationary phase may also account for the delayed accumulation of midcell signal during this phase (Figure 5F) relative to exponentially growth (Figure 5C).

DISCUSSION

We have undertaken this work to facilitate microscopy-based investigations of the biology of the Lyme disease agent *B. burgdorferi*. We expanded the available molecular toolkit by

characterizing antibiotic resistance markers, fluorescent proteins and constitutively active promoters not previously used in this organism.

Alongside the commonly used kanamycin, gentamicin, streptomycin, and erythromycin selection markers, the addition of hygromycin B and blasticidin S resistances as useful selection markers will provide more flexibility in designing genetic modifications. A wider array of non-cross-resistant selection markers is particularly important in the absence of a streamlined method to create unmarked genetic modifications in this bacterium (13). Currently, in infectious *B. burgdorferi* strains, an antibiotic resistance marker is commonly used to inactivate the restriction modification system encoded by the *bbe02* locus on plasmid lp25. This inactivation increases the efficiency of transformation with shuttle vectors. It also helps maintain this plasmid in the cell population during *in vitro* growth through selective pressure (78-81). This latter point is essential for maintaining a strain's infectivity, as linear plasmid lp25 is essential *in vivo,* but is often rapidly lost during genetic manipulations and growth in culture (82, 83). A second resistance marker is often used to inactivate a gene of interest, either by targeted deletion or by transposon insertion mutagenesis. A third resistance marker is needed for complementation, either at the original locus, or *in trans*. Additional markers are needed if two genes are to be inactivated and complemented simultaneously, or if several protein localization reporters need to be expressed both simultaneously and independently.

Today's cell biology investigations often rely on microscopy studies using fluorescent protein fusions. Prior to our work, green and red fluorescent proteins have been the reporters of choice in *B. burgdorferi* microscopy studies (Table 3), and only a handful of subcellular localization and lipoprotein topology studies had been performed using these tools (13-19). We have expanded the palette of fluorescent proteins that can be used in this bacterium by adding several proteins with properties highly desirable for imaging and localization studies. These fluorescent proteins are among the brightest of their classes (20, 40, 43), and their spectral

properties render them appropriate for simultaneous multi-color imaging of up to four targets. For the most part, they are also monomeric, as all of the *A. victoria* GFP, CFP, and YFP variants that we have generated carry the A206K mutation (41). Using monomeric fluorescent proteins may be important to prevent artifactual intermolecular interactions, (e.g., (41, 84, 85)). Should the weakly dimeric versions of these proteins be required for specific applications, the A206K mutation can be easily reversed by site-directed mutagenesis. Furthermore, the superfolder variants of these proteins may facilitate tagging when the folding of the fusion protein is otherwise impaired (40). In addition, unlike EGFP, which does not fold in the periplasm of diderm bacteria when exported through the Sec protein translocation system, sfGFP does fold in this compartment (86). It can therefore be an alternative to mRFP1 and mCherry for tagging periplasmic and outer surface-exposed proteins. This is particularly relevant for the study of *B. burgdorferi* since this bacterium expresses an unusually large number of lipoproteins that are localized on the cell surface or in the periplasmic space (87).

In addition, although dimeric, iRFP may serve as a useful *in vivo* marker, and may be preferable to GFP and RFP. Excitation light penetrance in live tissues is better in the far-red/near-infrared region of the spectrum than in the blue-shifted regions used to excite GFP and RFP. Furthermore, tissue autofluorescence in this spectral region is lower, which further facilitates imaging (88, 89). Lastly, the levels of biliverdin found in animal tissues are in the low milimolar range, with healthy human plasma containing 0.9-6.5 μM biliverdin (90). In our hands, such biliverdin levels are sufficient to elicit maximal fluorescence of *B. burgdorferi*-expressed iRFP. Furthermore, iRFP has been successfully used to label the bacterium *Neisseria meningitidis* for *in vivo* imaging (91). Altogether, these considerations suggest that imaging in mice using iRFP-expressing *B. burgdorferi* should be feasible.

We also characterized promoters of low and intermediate strengths and demonstrated that variable degrees of constitutive gene expression can be easily achieved in *B. burgdorferi*. The

relative order of promoter strength, as quantified using the mCherry reporter (Figure 3C), largely matched the order of the expression levels of the corresponding genes in culture (Figure 3A) (64), with the exceptions of P_{0526} and P_{0826}. While P_{0526} had an intermediate strength as measured by RNA-seq, it was the weakest when tested using our reporter system. In contrast, P_{0826} was the weakest promoter based on RNA-seq data, but displayed intermediate strength in our experiments. These differences may stem from strain differences or from our use of short DNA sequences of 129 to 212 bp, which presumably contain minimal promoter sequences. Any native regulatory elements located further upstream of these short promoter sequences are thus absent in our reporter plasmids. Differences in expression levels may also be caused by reporter expression from circular shuttle vectors. The native P_{0526} and P_{0826} sequences are located on the chromosome and differences in DNA topology, including supercoiling, between the chromosome and the circular plasmids are known to affect gene expression in *B. burgdorferi* (92, 93). Finally, it is worth noting that while both *bb0526* and *bb0826* encode leaderless transcripts, *bb0826* has a secondary transcriptional start site located 54 bp upstream of the translational start site (65). This difference may also partly explain the observed promoter strength mismatch between the native gene and reporter fusion. Regardless of the reason for these discrepancies, these promoters will facilitate complementation and localization studies where medium and low gene expression levels may be required.

To demonstrate the usefulness of these molecular reagents, we used them to generate and express an mCherry fusion to the LysM domain-containing protein BB0323. LysM domain-containing proteins, including BB0323, have been shown to bind the peptidoglycan layer (28, 94). Strikingly, BB0323-mCherry localized at the cellular poles and at future division sites at midcell throughout most of the cell cycle. Near the end of the cell cycle, before cells separate, BB0323-mCherry also often accumulated at 1/4 and 3/4 cell positions corresponding to the

division sites of future daughter cells. We previously demonstrated that the midcell and the 1/4 and 3/4 positions represent regions of active peptidoglycan synthesis in *B. burgdorferi* (6). Perhaps BB0323 accumulates at sites of peptidoglycan growth because they differ in chemical composition. A more likely alternative is that these peptidoglycan regions are multi-layered. A higher local peptidoglycan concentration would provide a denser binding platform for BB0323, resulting in its accumulation. In fact, cryo-electron tomography imaging of *B. burgdorferi* has revealed multiple layers of peptidoglycan at division sites (4), as well as a thick peptidoglycan layer at the poles (95). Accumulation of BB0323 at sites of multi-layered peptidoglycan would be reminiscent of the LysM-containing protein DipM in the α-proteobacterium *Caulobacter crescentus*, which localizes at zones of multi-layered peptidoglycan, including division sites and poles, via its LysM domains (96-98). Importantly, the striking cell cycle-coordinated localization of BB0323 demonstrates that proteins with critical functions are spatially distributed in *B. burgdorferi*, highlighting a layer of regulation that has been poorly explored in spirochetes.

In summary, our study describes novel molecular tools that we hope will aid investigations in the Lyme disease field and spur further progress in the study of this medically important and highly unusual bacterium.

DATA AVAILABILITY

Sequences of all the plasmids constructed in this study are available upon request. The DNA sequences of the various genes that were codon-optimized for expression in *B. burgdorferi* are provided in the Supplemental Material. The MATLAB code used to process cell fluorescence data is also provided as Supplemental Material.

ACCESSION NUMBERS

DNA sequences of codon-optimized genes have been deposited at GenBank under accession numbers MH644044 through MH644053.

SUPPLEMENTAL MATERIAL

Supplemental Material is available in the accompanying document. It contains detailed plasmid construction methods, a list of oligonucleotide primer sequences used in this study, DNA sequences of genes that were codon-optimized for translation in *B. burgdorferi*, a record of cell numbers for each figure describing quantitative fluorescence data, MATLAB code used in this study, and supplemental references.

ACKNOWLEDGEMENT

We thank Nicholas Jannetty for help with cloning experiments and Dr. Bradley Parry for help with the computational analyses. We are also grateful to Dr. Brandon Jutras and the members of the Jacobs-Wagner laboratory for helpful discussions and/or critical reading of the manuscript.

FUNDING

This work was supported by the Howard Hughes Medical Institute. C.J.-W. is an Investigator of the Howard Hughes Medical Institute. The funder had no role in study design, data collection and interpretation, or the decision to submit the work for publication. P.A.R. is a Senior Investigator supported by the Intramural Research Program of the National Institute of Allergy and Infectious Diseases, National Institutes of Health and contributed to this work while a Visiting Fellow in the C.J.-W. laboratory at Yale University.

CONFLICT OF INTEREST

The authors are aware of no conflict of interest.

REFERENCES

1. Mead PS. 2015. Epidemiology of Lyme disease. Infect Dis Clin North Am 29:187-210.
2. Steere AC, Strle F, Wormser GP, Hu LT, Branda JA, Hovius JW, Li X, Mead PS. 2016. Lyme borreliosis. Nat Rev Dis Primers 2:16090.
3. Holt SC. 1978. Anatomy and chemistry of spirochetes. Microbiol Rev 42:114-60.
4. Kudryashev M, Cyrklaff M, Baumeister W, Simon MM, Wallich R, Frischknecht F. 2009. Comparative cryo-electron tomography of pathogenic Lyme disease spirochetes. Mol Microbiol 71:1415-34.
5. Hovind-Hougen K. 1984. Ultrastructure of spirochetes isolated from Ixodes ricinus and Ixodes dammini. Yale J Biol Med 57:543-8.
6. Jutras BL, Scott M, Parry B, Biboy J, Gray J, Vollmer W, Jacobs-Wagner C. 2016. Lyme disease and relapsing fever Borrelia elongate through zones of peptidoglycan synthesis that mark division sites of daughter cells. Proc Natl Acad Sci U S A 113:9162-70.
7. Charon NW, Cockburn A, Li C, Liu J, Miller KA, Miller MR, Motaleb MA, Wolgemuth CW. 2012. The unique paradigm of spirochete motility and chemotaxis. Annu Rev Microbiol 66:349-70.
8. Motaleb MA, Corum L, Bono JL, Elias AF, Rosa P, Samuels DS, Charon NW. 2000. Borrelia burgdorferi periplasmic flagella have both skeletal and motility functions. Proc Natl Acad Sci U S A 97:10899-904.
9. Fraser CM, Casjens S, Huang WM, Sutton GG, Clayton R, Lathigra R, White O, Ketchum KA, Dodson R, Hickey EK, Gwinn M, Dougherty B, Tomb JF, Fleischmann RD, Richardson D, Peterson J, Kerlavage AR, Quackenbush J, Salzberg S, Hanson M, van Vugt R, Palmer N, Adams MD, Gocayne J, Weidman J, Utterback T, Watthey L, McDonald L, Artiach P, Bowman C, Garland S, Fuji C, Cotton MD, Horst K, Roberts K, Hatch B, Smith HO, Venter JC. 1997. Genomic sequence of a Lyme disease spirochaete, Borrelia burgdorferi. Nature 390:580-6.
10. Casjens S, Palmer N, van Vugt R, Huang WM, Stevenson B, Rosa P, Lathigra R, Sutton G, Peterson J, Dodson RJ, Haft D, Hickey E, Gwinn M, White O, Fraser CM. 2000. A bacterial genome in flux: the twelve linear and nine circular extrachromosomal DNAs in an infectious isolate of the Lyme disease spirochete Borrelia burgdorferi. Mol Microbiol 35:490-516.
11. Radolf JD, Caimano MJ, Stevenson B, Hu LT. 2012. Of ticks, mice and men: understanding the dual-host lifestyle of Lyme disease spirochaetes. Nat Rev Microbiol 10:87-99.
12. Rosa PA, Tilly K, Stewart PE. 2005. The burgeoning molecular genetics of the Lyme disease spirochaete. Nat Rev Microbiol 3:129-43.
13. Drecktrah D, Samuels DS. 2018. Genetic Manipulation of Borrelia Spp. Curr Top Microbiol Immunol 415:113-140.
14. Xu H, Raddi G, Liu J, Charon NW, Li C. 2011. Chemoreceptors and flagellar motors are subterminally located in close proximity at the two cell poles in spirochetes. J Bacteriol 193:2652-6.
15. Zhang K, Liu J, Charon NW, Li C. 2016. Hypothetical Protein BB0569 Is Essential for Chemotaxis of the Lyme Disease Spirochete Borrelia burgdorferi. J Bacteriol 198:664-72.
16. Li C, Xu H, Zhang K, Liang FT. 2010. Inactivation of a putative flagellar motor switch protein FliG1 prevents Borrelia burgdorferi from swimming in highly viscous media and blocks its infectivity. Mol Microbiol 75:1563-76.

17. Schulze RJ, Chen S, Kumru OS, Zuckert WR. 2010. Translocation of Borrelia burgdorferi surface lipoprotein OspA through the outer membrane requires an unfolded conformation and can initiate at the C-terminus. Mol Microbiol 76:1266-78.
18. Schulze RJ, Zuckert WR. 2006. Borrelia burgdorferi lipoproteins are secreted to the outer surface by default. Mol Microbiol 59:1473-84.
19. Kumru OS, Schulze RJ, Slusser JG, Zuckert WR. 2010. Development and validation of a FACS-based lipoprotein localization screen in the Lyme disease spirochete Borrelia burgdorferi. BMC Microbiol 10:277.
20. Chudakov DM, Matz MV, Lukyanov S, Lukyanov KA. 2010. Fluorescent proteins and their applications in imaging living cells and tissues. Physiol Rev 90:1103-63.
21. Wennmalm S, Simon SM. 2007. Studying individual events in biology. Annu Rev Biochem 76:419-46.
22. Yao Z, Carballido-Lopez R. 2014. Fluorescence imaging for bacterial cell biology: from localization to dynamics, from ensembles to single molecules. Annu Rev Microbiol 68:459-76.
23. Jacobs C, Domian IJ, Maddock JR, Shapiro L. 1999. Cell cycle-dependent polar localization of an essential bacterial histidine kinase that controls DNA replication and cell division. Cell 97:111-20.
24. Gordon GS, Sitnikov D, Webb CD, Teleman A, Straight A, Losick R, Murray AW, Wright A. 1997. Chromosome and low copy plasmid segregation in E. coli: visual evidence for distinct mechanisms. Cell 90:1113-21.
25. Arigoni F, Pogliano K, Webb CD, Stragier P, Losick R. 1995. Localization of protein implicated in establishment of cell type to sites of asymmetric division. Science 270:637-40.
26. Stewart PE, Hoff J, Fischer E, Krum JG, Rosa PA. 2004. Genome-wide transposon mutagenesis of Borrelia burgdorferi for identification of phenotypic mutants. Appl Environ Microbiol 70:5973-9.
27. Zhang X, Yang X, Kumar M, Pal U. 2009. BB0323 function is essential for Borrelia burgdorferi virulence and persistence through tick-rodent transmission cycle. J Infect Dis 200:1318-30.
28. Kariu T, Yang X, Marks CB, Zhang X, Pal U. 2013. Proteolysis of BB0323 results in two polypeptides that impact physiologic and infectious phenotypes in Borrelia burgdorferi. Mol Microbiol 88:510-22.
29. Barbour AG. 1984. Isolation and cultivation of Lyme disease spirochetes. Yale J Biol Med 57:521-5.
30. Zuckert WR. 2007. Laboratory maintenance of Borrelia burgdorferi. Curr Protoc Microbiol Chapter 12:Unit 12C 1.
31. Jutras BL, Chenail AM, Stevenson B. 2013. Changes in bacterial growth rate govern expression of the Borrelia burgdorferi OspC and Erp infection-associated surface proteins. J Bacteriol 195:757-64.
32. Samuels DS. 1995. Electrotransformation of the spirochete Borrelia burgdorferi. Methods Mol Biol 47:253-9.
33. Grote A, Hiller K, Scheer M, Munch R, Nortemann B, Hempel DC, Jahn D. 2005. JCat: a novel tool to adapt codon usage of a target gene to its potential expression host. Nucleic Acids Res 33:W526-31.
34. Nakamura Y, Gojobori T, Ikemura T. 2000. Codon usage tabulated from international DNA sequence databases: status for the year 2000. Nucleic Acids Res 28:292.
35. Glaser P, Sharpe ME, Raether B, Perego M, Ohlsen K, Errington J. 1997. Dynamic, mitotic-like behavior of a bacterial protein required for accurate chromosome partitioning. Genes Dev 11:1160-8.
36. Paintdakhi A, Parry B, Campos M, Irnov I, Elf J, Surovtsev I, Jacobs-Wagner C. 2016. Oufti: an integrated software package for high-accuracy, high-throughput quantitative microscopy analysis. Mol Microbiol 99:767-77.
37. Rizzo MA, Springer GH, Granada B, Piston DW. 2004. An improved cyan fluorescent protein variant useful for FRET. Nat Biotechnol 22:445-9.
38. Yang TT, Cheng L, Kain SR. 1996. Optimized codon usage and chromophore mutations provide enhanced sensitivity with the green fluorescent protein. Nucleic Acids Res 24:4592-3.

39. Griesbeck O, Baird GS, Campbell RE, Zacharias DA, Tsien RY. 2001. Reducing the environmental sensitivity of yellow fluorescent protein. Mechanism and applications. J Biol Chem 276:29188-94.
40. Pedelacq JD, Cabantous S, Tran T, Terwilliger TC, Waldo GS. 2006. Engineering and characterization of a superfolder green fluorescent protein. Nat Biotechnol 24:79-88.
41. Zacharias DA, Violin JD, Newton AC, Tsien RY. 2002. Partitioning of lipid-modified monomeric GFPs into membrane microdomains of live cells. Science 296:913-6.
42. Shaner NC, Campbell RE, Steinbach PA, Giepmans BN, Palmer AE, Tsien RY. 2004. Improved monomeric red, orange and yellow fluorescent proteins derived from Discosoma sp. red fluorescent protein. Nat Biotechnol 22:1567-72.
43. Filonov GS, Piatkevich KD, Ting LM, Zhang J, Kim K, Verkhusha VV. 2011. Bright and stable near-infrared fluorescent protein for in vivo imaging. Nat Biotechnol 29:757-61.
44. Rodriguez EA, Campbell RE, Lin JY, Lin MZ, Miyawaki A, Palmer AE, Shu X, Zhang J, Tsien RY. 2017. The Growing and Glowing Toolbox of Fluorescent and Photoactive Proteins. Trends Biochem Sci 42:111-129.
45. Bono JL, Elias AF, Kupko JJ, 3rd, Stevenson B, Tilly K, Rosa P. 2000. Efficient targeted mutagenesis in Borrelia burgdorferi. J Bacteriol 182:2445-52.
46. Dunham-Ems SM, Caimano MJ, Pal U, Wolgemuth CW, Eggers CH, Balic A, Radolf JD. 2009. Live imaging reveals a biphasic mode of dissemination of Borrelia burgdorferi within ticks. J Clin Invest 119:3652-65.
47. Moriarty TJ, Norman MU, Colarusso P, Bankhead T, Kubes P, Chaconas G. 2008. Real-time high resolution 3D imaging of the lyme disease spirochete adhering to and escaping from the vasculature of a living host. PLoS Pathog 4:e1000090.
48. Hyde JA, Weening EH, Chang M, Trzeciakowski JP, Hook M, Cirillo JD, Skare JT. 2011. Bioluminescent imaging of Borrelia burgdorferi in vivo demonstrates that the fibronectin-binding protein BBK32 is required for optimal infectivity. Mol Microbiol 82:99-113.
49. Lybarger SR, Johnson TL, Gray MD, Sikora AE, Sandkvist M. 2009. Docking and assembly of the type II secretion complex of Vibrio cholerae. J Bacteriol 191:3149-61.
50. Montero Llopis P, Jackson AF, Sliusarenko O, Surovtsev I, Heinritz J, Emonet T, Jacobs-Wagner C. 2010. Spatial organization of the flow of genetic information in bacteria. Nature 466:77-81.
51. von Schwedler UK, Stuchell M, Muller B, Ward DM, Chung HY, Morita E, Wang HE, Davis T, He GP, Cimbora DM, Scott A, Krausslich HG, Kaplan J, Morham SG, Sundquist WI. 2003. The protein network of HIV budding. Cell 114:701-13.
52. Zamborlini A, Usami Y, Radoshitzky SR, Popova E, Palu G, Gottlinger H. 2006. Release of autoinhibition converts ESCRT-III components into potent inhibitors of HIV-1 budding. Proc Natl Acad Sci U S A 103:19140-5.
53. Goila-Gaur R, Demirov DG, Orenstein JM, Ono A, Freed EO. 2003. Defects in human immunodeficiency virus budding and endosomal sorting induced by TSG101 overexpression. J Virol 77:6507-19.
54. Strack B, Calistri A, Craig S, Popova E, Gottlinger HG. 2003. AIP1/ALIX is a binding partner for HIV-1 p6 and EIAV p9 functioning in virus budding. Cell 114:689-99.
55. Martin-Serrano J, Yarovoy A, Perez-Caballero D, Bieniasz PD. 2003. Divergent retroviral late-budding domains recruit vacuolar protein sorting factors by using alternative adaptor proteins. Proc Natl Acad Sci U S A 100:12414-9.
56. Lin Y, Kimpler LA, Naismith TV, Lauer JM, Hanson PI. 2005. Interaction of the mammalian endosomal sorting complex required for transport (ESCRT) III protein hSnf7-1 with itself, membranes, and the AAA+ ATPase SKD1. J Biol Chem 280:12799-809.
57. Howard TL, Stauffer DR, Degnin CR, Hollenberg SM. 2001. CHMP1 functions as a member of a newly defined family of vesicle trafficking proteins. J Cell Sci 114:2395-404.

58. Broder DH, Pogliano K. 2006. Forespore engulfment mediated by a ratchet-like mechanism. Cell 126:917-28.
59. Gregory JA, Becker EC, Pogliano K. 2008. Bacillus subtilis MinC destabilizes FtsZ-rings at new cell poles and contributes to the timing of cell division. Genes Dev 22:3475-88.
60. Jouvenet N, Simon SM, Bieniasz PD. 2009. Imaging the interaction of HIV-1 genomes and Gag during assembly of individual viral particles. Proc Natl Acad Sci U S A 106:19114-9.
61. Jouvenet N, Zhadina M, Bieniasz PD, Simon SM. 2011. Dynamics of ESCRT protein recruitment during retroviral assembly. Nat Cell Biol 13:394-401.
62. Bleck M, Itano MS, Johnson DS, Thomas VK, North AJ, Bieniasz PD, Simon SM. 2014. Temporal and spatial organization of ESCRT protein recruitment during HIV-1 budding. Proc Natl Acad Sci U S A 111:12211-6.
63. Itano MS, Bleck M, Johnson DS, Simon SM. 2016. Readily Accessible Multiplane Microscopy: 3D Tracking the HIV-1 Genome in Living Cells. Traffic 17:179-86.
64. Arnold WK, Savage CR, Brissette CA, Seshu J, Livny J, Stevenson B. 2016. RNA-Seq of Borrelia burgdorferi in Multiple Phases of Growth Reveals Insights into the Dynamics of Gene Expression, Transcriptome Architecture, and Noncoding RNAs. PLoS One 11:e0164165.
65. Adams PP, Flores Avile C, Popitsch N, Bilusic I, Schroeder R, Lybecker M, Jewett MW. 2017. In vivo expression technology and 5' end mapping of the Borrelia burgdorferi transcriptome identify novel RNAs expressed during mammalian infection. Nucleic Acids Res 45:775-792.
66. Frank KL, Bundle SF, Kresge ME, Eggers CH, Samuels DS. 2003. aadA confers streptomycin resistance in Borrelia burgdorferi. J Bacteriol 185:6723-7.
67. Elias AF, Bono JL, Kupko JJ, 3rd, Stewart PE, Krum JG, Rosa PA. 2003. New antibiotic resistance cassettes suitable for genetic studies in Borrelia burgdorferi. J Mol Microbiol Biotechnol 6:29-40.
68. Sartakova M, Dobrikova E, Cabello FC. 2000. Development of an extrachromosomal cloning vector system for use in Borrelia burgdorferi. Proc Natl Acad Sci U S A 97:4850-5.
69. Kimura M, Kamakura T, Tao QZ, Kaneko I, Yamaguchi I. 1994. Cloning of the blasticidin S deaminase gene (BSD) from Aspergillus terreus and its use as a selectable marker for Schizosaccharomyces pombe and Pyricularia oryzae. Mol Gen Genet 242:121-9.
70. Gritz L, Davies J. 1983. Plasmid-encoded hygromycin B resistance: the sequence of hygromycin B phosphotransferase gene and its expression in Escherichia coli and Saccharomyces cerevisiae. Gene 25:179-88.
71. Rao RN, Allen NE, Hobbs JN, Jr., Alborn WE, Jr., Kirst HA, Paschal JW. 1983. Genetic and enzymatic basis of hygromycin B resistance in Escherichia coli. Antimicrob Agents Chemother 24:689-95.
72. Thanbichler M, Iniesta AA, Shapiro L. 2007. A comprehensive set of plasmids for vanillate- and xylose-inducible gene expression in Caulobacter crescentus. Nucleic Acids Res 35:e137.
73. Qin A, Tucker AM, Hines A, Wood DO. 2004. Transposon mutagenesis of the obligate intracellular pathogen Rickettsia prowazekii. Appl Environ Microbiol 70:2816-22.
74. Tribuddharat C, Fennewald M. 1999. Integron-mediated rifampin resistance in Pseudomonas aeruginosa. Antimicrob Agents Chemother 43:960-2.
75. Johnson SE, Klein GC, Schmid GP, Feeley JC. 1984. Susceptibility of the Lyme disease spirochete to seven antimicrobial agents. Yale J Biol Med 57:549-53.
76. Alekshun M, Kashlev M, Schwartz I. 1997. Molecular cloning and characterization of Borrelia burgdorferi rpoB. Gene 186:227-35.
77. Ostberg Y, Carroll JA, Pinne M, Krum JG, Rosa P, Bergstrom S. 2004. Pleiotropic effects of inactivating a carboxyl-terminal protease, CtpA, in Borrelia burgdorferi. J Bacteriol 186:2074-84.
78. Chan K, Alter L, Barthold SW, Parveen N. 2015. Disruption of bbe02 by Insertion of a Luciferase Gene Increases Transformation Efficiency of Borrelia burgdorferi and Allows Live Imaging in Lyme Disease Susceptible C3H Mice. PLoS One 10:e0129532.

79. Rego RO, Bestor A, Rosa PA. 2011. Defining the plasmid-borne restriction-modification systems of the Lyme disease spirochete Borrelia burgdorferi. J Bacteriol 193:1161-71.
80. Kawabata H, Norris SJ, Watanabe H. 2004. BBE02 disruption mutants of Borrelia burgdorferi B31 have a highly transformable, infectious phenotype. Infect Immun 72:7147-54.
81. Lawrenz MB, Kawabata H, Purser JE, Norris SJ. 2002. Decreased electroporation efficiency in Borrelia burgdorferi containing linear plasmids lp25 and lp56: impact on transformation of infectious B. burgdorferi. Infect Immun 70:4798-804.
82. Purser JE, Norris SJ. 2000. Correlation between plasmid content and infectivity in Borrelia burgdorferi. Proc Natl Acad Sci U S A 97:13865-70.
83. Labandeira-Rey M, Skare JT. 2001. Decreased infectivity in Borrelia burgdorferi strain B31 is associated with loss of linear plasmid 25 or 28-1. Infect Immun 69:446-55.
84. Landgraf D, Okumus B, Chien P, Baker TA, Paulsson J. 2012. Segregation of molecules at cell division reveals native protein localization. Nat Methods 9:480-2.
85. Wang S, Moffitt JR, Dempsey GT, Xie XS, Zhuang X. 2014. Characterization and development of photoactivatable fluorescent proteins for single-molecule-based superresolution imaging. Proc Natl Acad Sci U S A 111:8452-7.
86. Dinh T, Bernhardt TG. 2011. Using superfolder green fluorescent protein for periplasmic protein localization studies. J Bacteriol 193:4984-7.
87. Dowdell AS, Murphy MD, Azodi C, Swanson SK, Florens L, Chen S, Zuckert WR. 2017. Comprehensive Spatial Analysis of the Borrelia burgdorferi Lipoproteome Reveals a Compartmentalization Bias toward the Bacterial Surface. J Bacteriol 199:e00658-16.
88. Weissleder R, Ntziachristos V. 2003. Shedding light onto live molecular targets. Nat Med 9:123-8.
89. Jobsis FF. 1977. Noninvasive, infrared monitoring of cerebral and myocardial oxygen sufficiency and circulatory parameters. Science 198:1264-7.
90. Gafvels M, Holmstrom P, Somell A, Sjovall F, Svensson JO, Stahle L, Broome U, Stal P. 2009. A novel mutation in the biliverdin reductase-A gene combined with liver cirrhosis results in hyperbiliverdinaemia (green jaundice). Liver Int 29:1116-24.
91. Bonazzi D, Lo Schiavo V, Machata S, Djafer-Cherif I, Nivoit P, Manriquez V, Tanimoto H, Husson J, Henry N, Chate H, Voituriez R, Dumenil G. 2018. Intermittent Pili-Mediated Forces Fluidize Neisseria meningitidis Aggregates Promoting Vascular Colonization. Cell 174:143-155 e16.
92. Alverson J, Bundle SF, Sohaskey CD, Lybecker MC, Samuels DS. 2003. Transcriptional regulation of the ospAB and ospC promoters from Borrelia burgdorferi. Mol Microbiol 48:1665-77.
93. Alverson J, Samuels DS. 2002. groEL expression in gyrB mutants of Borrelia burgdorferi. J Bacteriol 184:6069-72.
94. Buist G, Steen A, Kok J, Kuipers OP. 2008. LysM, a widely distributed protein motif for binding to (peptido)glycans. Mol Microbiol 68:838-47.
95. Liu J, Lin T, Botkin DJ, McCrum E, Winkler H, Norris SJ. 2009. Intact flagellar motor of Borrelia burgdorferi revealed by cryo-electron tomography: evidence for stator ring curvature and rotor/C-ring assembly flexion. J Bacteriol 191:5026-36.
96. Goley ED, Comolli LR, Fero KE, Downing KH, Shapiro L. 2010. DipM links peptidoglycan remodelling to outer membrane organization in Caulobacter. Mol Microbiol 77:56-73.
97. Poggio S, Takacs CN, Vollmer W, Jacobs-Wagner C. 2010. A protein critical for cell constriction in the Gram-negative bacterium Caulobacter crescentus localizes at the division site through its peptidoglycan-binding LysM domains. Mol Microbiol 77:74-89.
98. Moll A, Schlimpert S, Briegel A, Jensen GJ, Thanbichler M. 2010. DipM, a new factor required for peptidoglycan remodelling during cell division in Caulobacter crescentus. Mol Microbiol 77:90-107.
99. Elias AF, Stewart PE, Grimm D, Caimano MJ, Eggers CH, Tilly K, Bono JL, Akins DR, Radolf JD, Schwan TG, Rosa P. 2002. Clonal polymorphism of Borrelia burgdorferi strain B31 MI: implications for mutagenesis in an infectious strain background. Infect Immun 70:2139-50.

100. Casjens S, van Vugt R, Tilly K, Rosa PA, Stevenson B. 1997. Homology throughout the multiple 32-kilobase circular plasmids present in Lyme disease spirochetes. J Bacteriol 179:217-27.
101. Jewett MW, Byram R, Bestor A, Tilly K, Lawrence K, Burtnick MN, Gherardini F, Rosa PA. 2007. Genetic basis for retention of a critical virulence plasmid of Borrelia burgdorferi. Mol Microbiol 66:975-90.
102. Babb K, McAlister JD, Miller JC, Stevenson B. 2004. Molecular characterization of Borrelia burgdorferi erp promoter/operator elements. J Bacteriol 186:2745-56.
103. Stewart PE, Thalken R, Bono JL, Rosa P. 2001. Isolation of a circular plasmid region sufficient for autonomous replication and transformation of infectious Borrelia burgdorferi. Mol Microbiol 39:714-21.
104. Miller WG, Bates AH, Horn ST, Brandl MT, Wachtel MR, Mandrell RE. 2000. Detection on surfaces and in Caco-2 cells of Campylobacter jejuni cells transformed with new gfp, yfp, and cfp marker plasmids. Appl Environ Microbiol 66:5426-36.
105. Eggers CH, Caimano MJ, Clawson ML, Miller WG, Samuels DS, Radolf JD. 2002. Identification of loci critical for replication and compatibility of a Borrelia burgdorferi cp32 plasmid and use of a cp32-based shuttle vector for the expression of fluorescent reporters in the lyme disease spirochaete. Mol Microbiol 43:281-95.
106. Cormack BP, Valdivia RH, Falkow S. 1996. FACS-optimized mutants of the green fluorescent protein (GFP). Gene 173:33-8.
107. Miller WG, Leveau JH, Lindow SE. 2000. Improved gfp and inaZ broad-host-range promoter-probe vectors. Mol Plant Microbe Interact 13:1243-50.
108. Miller WG, Lindow SE. 1997. An improved GFP cloning cassette designed for prokaryotic transcriptional fusions. Gene 191:149-53.
109. Crameri A, Whitehorn EA, Tate E, Stemmer WP. 1996. Improved green fluorescent protein by molecular evolution using DNA shuffling. Nat Biotechnol 14:315-9.
110. Carroll JA, Stewart PE, Rosa P, Elias AF, Garon CF. 2003. An enhanced GFP reporter system to monitor gene expression in Borrelia burgdorferi. Microbiology 149:1819-28.
111. Campbell RE, Tour O, Palmer AE, Steinbach PA, Baird GS, Zacharias DA, Tsien RY. 2002. A monomeric red fluorescent protein. Proc Natl Acad Sci U S A 99:7877-82.
112. Lee WY, Moriarty TJ, Wong CH, Zhou H, Strieter RM, van Rooijen N, Chaconas G, Kubes P. 2010. An intravascular immune response to Borrelia burgdorferi involves Kupffer cells and iNKT cells. Nat Immunol 11:295-302.
113. Sartakova ML, Dobrikova EY, Terekhova DA, Devis R, Bugrysheva JV, Morozova OV, Godfrey HP, Cabello FC. 2003. Novel antibiotic-resistance markers in pGK12-derived vectors for Borrelia burgdorferi. Gene 303:131-7.
114. Terekhova D, Sartakova ML, Wormser GP, Schwartz I, Cabello FC. 2002. Erythromycin resistance in Borrelia burgdorferi. Antimicrob Agents Chemother 46:3637-40.

FIGURES LEGENDS

Figure 1. Fluorescent protein characterization. A. *B. burgdorferi* strains CJW_Bb090 through CJW_Bb096 expressing the indicated fluorescent proteins were imaged with matching filter sets. **B.** Strain CJW_Bb100 expressing iRFP requires biliverdin for development of fluorescence. Cells were grown in liquid culture with biliverdin for two days prior to imaging using a Cy5.5 filter set. **C.** Dose-response of iRFP fluorescence to biliverdin concentration. Strain CJW_Bb100 was grown in the presence of biliverdin for two days prior to imaging. Between 86 and 206 cells were analyzed for each concentration. Total cellular fluorescence levels were normalized by the cell area. Shown are means ± standard deviations (SD). A.U., arbitrary units. **D.** Time-course of iRFP fluorescence development in strain CJW_Bb100 following addition of 16 μM biliverdin. Between 68 and 110 cells were analyzed for each time point. **E.** Biliverdin does not affect *B. burgdorferi* growth. Strain CJW_Bb100 was inoculated at 10^4 cells/mL in duplicate in medium containing 4 μM biliverdin or no biliverdin, after which the spirochetes were enumerated daily.

Figure 2. Quantification of fluorescent protein signal using common fluorescence filter sets. Strains CJW_Bb090 through CJW_Bb096 and CJW_Bb100 expressing the fluorescent proteins indicated at the bottom of the figure were each imaged using five filter sets: CFP, GFP, YFP, mCherry/TexasRed, and Cy5.5 (see the Materials and Methods section for filter set specifications). Strain CJW_Bb073 carrying an empty shuttle vector (EV) was also imaged to measure the cellular autofluorescence. Each filter set is listed at the top of the corresponding graph. Fluorescence intensity values were normalized by the cell area and are depicted as means ± SD in arbitrary units (A.U.). For each strain, 117 to 308 cells were analyzed. The iRFP strain was grown in the presence of 4 μM biliverdin for three days prior to imaging. The

boxed region in each plot highlights the data obtained with filter sets that were ideal for the expressed fluorescent protein.

Figure 3. Promoter strength quantification. A. mRNA expression levels extracted from published RNA-seq data obtained using strain B31-A3 (99) grown to early exponential phase (10^6 cells/mL), mid-exponential phase (10^7 cells/mL), or stationary phase (one day after reaching 10^8 cells/mL) (64). FPKM, fragments per kilobase transcript per million mapped reads. **B.** Promoter reporter plasmid map (not drawn to scale). IR, inverted repeats; cp9 *ori*, origin of replication of *B. burgdorferi* plasmid cp9, which includes the genes *orf1*, *orf2*, *orf3* needed for plasmid replication in *B. burgdorferi*; colE1 *ori*, *E. coli* origin of replication; P_{flgB}, *B. burgdorferi* flagellar rod operon promoter; *aphI*, kanamycin resistance gene. The promoter (blue) and the mCherry-coding sequence (red) are connected by a BamHI restriction enzyme site and a ribosomal binding site (RBS). The native locus from which the promoter was extracted is depicted below the plasmid map. The BamHI-RBS-mCherry sequence effectively replaced the native gene's protein coding sequence (shown in pink). Translational START sites are marked by the ATG codon. **C.** Promoter strength quantified by measuring cellular mCherry fluorescence in strains CJW_Bb069, CJW_Bb108 through CJW_Bb112, and CJW_Bb146. The fluorescence levels were normalized by cell area. The promoters were ranked in increasing order of the mean fluorescence values and are listed below the graph. Shown are means ± SD. Between 97 and 160 cells were analyzed per strain. EV, empty vector; A.U., arbitrary units.

Figure 4. Characterization of blasticidin S and hygromycin B resistances in *B. burgdorferi*. A. Maps of shuttle vectors pBSV2B and pBSV2H. IR, inverted repeats; cp9 *ori*, origin or replication of *B. burgdorferi* plasmid cp9; colE1 *ori*, *E. coli* origin of replication; MCS, multicloning site; *arr-2*, rifampicin resistance gene for selection in *E. coli*; P_{flgB}, *B. burgdorferi*

flagellar rod operon promoter; *bsd*^{Bb}, *B. burgdorferi* codon-optimized blasticidin S deaminase-encoding gene; *hph*^{Bb}, *B. burgdorferi* codon-optimized hygromycin B phosphotransferase-encoding gene. The maps are not drawn to scale. **B.** Plate map showing the final antibiotic concentrations used for cross-resistance testing. Each concentration was tested in two adjacent wells. Concentrations routinely used for selection are indicated by the arrow. **C.** Schematic representation of color change of the growth medium from red (absence of spirochete growth) to orange/yellow (presence of spirochete growth). A line marks the boundary between growth and no growth in an antibiotic concentration series. The lowest antibiotic concentration that blocked growth was identified as the minimal inhibitory concentration (MIC). **D.-H.** Susceptibility test of each resistance-carrying strain to various antibiotic concentrations according to the plate layout shown in B. The plates were incubated to allow for growth-dependent acidification of the medium and change in phenol red pH indicator color from red to orange and yellow, as depicted in panel C. Images were obtained using colorimetric imaging of the individual plates. MIC boundaries are marked by dark lines. The strains used are listed above each image.

Figure 5. Localization of BB0323 using an mCherry fusion. A. Micrographs of cells of strain CJW_Bb173 imaged in exponential phase. Shown are mCherry fluorescence and phase contrast images. All images have the same magnification. Signal accumulation patterns are as follows: i, bipolar; ii, bipolar and midcell in the absence of obvious constriction in the phase contrast image; iii, bipolar and midcell in the presence of midcell constriction; and iv, bipolar, midcell in the presence of deep cell constriction, and at 1/4 and 3/4 positions along the cell length. **B.** Signal quantification along the cell length for cells shown in panel A. The mCherry signal is depicted in red, while the phase contrast signal is shown in gray. **A** and **B**. Polar localizations and midcell localizations flanking a deep constriction site are marked by filled red

arrowheads. Midcell localizations are otherwise marked by empty red arrowheads. Indentation in the phase contrast signal is marked by blue arrowheads. **C.** Demograph depicting the localization of BB0323-mCherry in a population of exponentially growing cells of strain CJW_Bb173. See text for a detailed description. i-iv depict the regions on the demograph where cells with the localization patterns highlighted in panels A and B are located. **D**. Micrographs of cells of strain CJW_Bb173 imaged in stationary phase. Shown are mCherry fluorescence and phase contrast images. All images have the same magnification. Signal accumulation patterns are as follows: i, bipolar; ii, bipolar and midcell in the absence of cell constriction in the phase contrast image; and iii, bipolar and midcell in the presence of midcell constriction. **E.** Signal quantification as a function of cell length for cells shown in panel D. The mCherry signal is depicted in red, while the phase contrast signal is shown in gray. D and E. Filled and empty red arrowheads mark polar and midcell localization, respectively, whereas the blue arrowhead shows cell constriction. **F.** Demograph depicting the localization of BB0323-mCherry in a stationary phase population of cells of strain CJW_Bb173. i-iii depict the regions on the demograph where cells with the localization patterns highlighted in panels D and E are located.

TABLES

Table 1. Strains used in this study

Strain	Genotype / description	Antibiotic resistance	Source or reference
***E. coli* cloning strains**			
DH5α	F^- Φ80*dlacZ*Δ*M15* Δ(*lacZYA-argF*) U169 *deoR recA1 endA1 hsdR17* (r_k^-, m_k^+) *phoA supE44* λ⁻*thi-1 gyrA96 relA1*	None	Promega
XL10-Gold	Tet^rΔ(*mcrA*)*183* Δ(*mcrCB-hsdSMR-mrr*)*173 endA1 supE44 thi⁻1 recA1 gyrA96 relA1 lac* Hte [F´ *proAB lacI*^{q}*Z*Δ*M15* Tn*10* (Tet^r) Amy Cam^r]	Tetracycline Chloramphenicol	Agilent
***B. burgdorferi* strains**			
B31 MI	Low-passage derivative of the type strain B31	None	(9)
B31 e2	Reduced genome non-infectious clone of strain B31	None	(100)
B31 A34	Reduced genome non-infectious clone of strain B31	None	(101)
CJW_Bb069	B31 e2 / pBSV2_2	Kanamycin	This study
CJW_Bb070	B31 e2 / pKFSS1_2	Streptomycin	This study
CJW_Bb071	B31 e2 / pBSV2H	Hygromycin B	This study
CJW_Bb072	B31 e2 / pBSV2B	Blasticidin S	This study
CJW_Bb073	B31 e2 / pBSV2G_2	Gentamicin	This study
CJW_Bb090	B31 e2 / pBSV2G_P_{flaB}-msfGFP^{Bb}	Gentamicin	This study
CJW_Bb091	B31 e2 / pBSV2G_P_{flaB}-msfCFP^{Bb}	Gentamicin	This study
CJW_Bb092	B31 e2 / pBSV2G_P_{flaB}-msfYFP^{Bb}	Gentamicin	This study
CJW_Bb093	B31 e2 / pBSV2G_P_{flaB}-mCherry^{Bb}	Gentamicin	This study
CJW_Bb094	B31 e2 / pBSV2G_P_{flaB}-mEGFP^{Bb}	Gentamicin	This study
CJW_Bb095	B31 e2 / pBSV2G_P_{flaB}-mCerulean^{Bb}	Gentamicin	This study
CJW_Bb096	B31 e2 / pBSV2G_P_{flaB}-mCitrine^{Bb}	Gentamicin	This study
CJW_Bb100	B31 e2 / pBSV2G_P_{flaB}-iRFP^{Bb}	Gentamicin	This study
CJW_Bb108	B31 e2 / pBSV2_P_{resT}-mCherry^{Bb}	Kanamycin	This study
CJW_Bb109	B31 e2 / pBSV2_P_{0026}-mCherry^{Bb}	Kanamycin	This study
CJW_Bb110	B31 e2 / pBSV2_P_{0031}-mCherry^{Bb}	Kanamycin	This study
CJW_Bb111	B31 e2 / pBSV2_P_{0526}-mCherry^{Bb}	Kanamycin	This study
CJW_Bb112	B31 e2 / pBSV2_P_{0826}-mCherry^{Bb}	Kanamycin	This study
CJW_Bb146	B31 e2 / pBSV2_P_{flaB}-mCherry^{Bb}	Kanamycin	This study
CJW_Bb173	B31 A34 / pBSV2G_P_{0826}-BB0323-mCherry^{Bb}	Gentamicin	This study

894

Table 2. Plasmids used in this study.

Plasmid name	Description	Antibiotic resistance	Reference
pBSV2G	Gentamicin-resistant *B. burgdorferi* shuttle vector	Gentamicin	(67)
pBLS599	pBSV2-derived *B. burgdorferi* shuttle vector lacking the zeocin gene; expresses *gfpmut3*	Kanamycin	(102)
pKFSS1	Streptomycin-resistant *B. burgdorferi* shuttle vector	Streptomycin	(66)
pMCS-3	Plasmid carrying the rifampicin resistance gene *arr-2*	Rifampicin	(72)
pSL1180	Ampicillin-resistant cloning plasmid	Ampicillin	Amersham
pBSV2G_2	Modified gentamicin-resistant *B. burgdorferi* shuttle vector; has extended multicloning site	Gentamicin	This study
pBSV2_2	Kanamycin-resistant *B. burgdorferi* shuttle vector similar to pBSV2 (103); lacks the zeocin gene; has extended multicloning site	Kanamycin	This study
pKFSS1_2	Modified streptomycin-resistant *B. burgdorferi* shuttle vector; has extended multicloning site	Streptomycin	This study
pBSV2B	Blasticidin S-resistant *B. burgdorferi* shuttle vector; uses rifampicin for selection in *E. coli*	Blasticidin S Rifampicin	This study
pBSV2H	Hygromycin B-resistant *B. burgdorferi* shuttle vector; uses rifampicin for selection in *E. coli*	Hygromycin B Rifampicin	This study
pBSV2G_P_{flaB}-mCherry^{Bb}	For expression of mCherry^{Bb} under the control of the strong *B. burgdorferi* promoter P_{flaB}	Gentamicin	This study
pBSV2G_P_{flaB}-msfGFP^{Bb}	For expression of msfGFP^{Bb} under the control of the strong *B. burgdorferi* promoter P_{flaB}	Gentamicin	This study
pBSV2G_P_{flaB}-msfCFP^{Bb}	For expression of msfCFP^{Bb} under the control of the strong *B. burgdorferi* promoter P_{flaB}	Gentamicin	This study
pBSV2G_P_{flaB}-msfYFP^{Bb}	For expression of msfYFP^{Bb} under the control of the strong *B. burgdorferi* promoter P_{flaB}	Gentamicin	This study
pBSV2G_P_{flaB}-mEGFP^{Bb}	For expression of mEGFP^{Bb} under the control of the strong *B. burgdorferi* promoter P_{flaB}	Gentamicin	This study
pBSV2G_P_{flaB}-mCerulean^{Bb}	For expression of mCerulean^{Bb} under the control of the strong *B. burgdorferi* promoter P_{flaB}	Gentamicin	This study
pBSV2G_P_{flaB}-mCitrine^{Bb}	For expression of mCitrine^{Bb} under the control of the strong *B. burgdorferi* promoter P_{flaB}	Gentamicin	This study
pBSV2G_P_{flaB}-iRFP^{Bb}	For expression of iRFP^{Bb} under the control of the strong *B. burgdorferi* promoter P_{flaB}	Gentamicin	This study
pBSV2_P_{resT}-mCherry^{Bb}	For expression of mCherry^{Bb} under the control of the *B. burgdorferi* promoter P_{resT}	Kanamycin	This study
pBSV2_P_{0026}-mCherry^{Bb}	For expression of mCherry^{Bb} under the control of the *B. burgdorferi* promoter P_{0026}	Kanamycin	This study
pBSV2_P_{0031}-mCherry^{Bb}	For expression of mCherry^{Bb} under the control of the *B. burgdorferi* promoter P_{0031}	Kanamycin	This study
pBSV2_P_{0526}-mCherry^{Bb}	For expression of mCherry^{Bb} under the control of the *B. burgdorferi* promoter P_{0526}	Kanamycin	This study
pBSV2_P_{0826}-mCherry^{Bb}	For expression of mCherry^{Bb} under the control of the *B. burgdorferi* promoter P_{0826}	Kanamycin	This study
pBSV2_P_{flaB}-mCherry^{Bb}	For expression of mCherry^{Bb} under the control of the strong *B. burgdorferi* promoter P_{flaB}	Kanamycin	This study
pBSV2G_P_{0826}-BB0323-mCherry^{Bb}	For expression of a BB0323-mCherry fusion under the control of the *B. burgdorferi* promoter P_{0826}	Gentamicin	This study

895

896

Table 3. Fluorescent proteins used in *B. burgdorferi*

Color class	Protein expressed	Ex/Em[a] max (nm)	Source or reference for protein/gene development	Reference for use in *B. burgdorferi*	Notes
I. Fluorescent proteins previously used in *B. burgdorferi:*					
Cyan	CFP	434/477[b]	Clontech; (104)	(105)	Rarely used
Green	EGFP	489/509	Clontech; (38)	(68)	Low expression; has mammalian codon usage
	GFPmut1	488/507	(104, 106-108)	(105)	Widely used; adapted for bacterial expression; same protein as EGFP
	GFPmut3	501/511	(106)	(102)	
	GFP cycle 3	NR[c]	(109)	(110)	Retains UV excitation peak
Yellow	YFP	514/527[b]	(104)	(105)	Rarely used
Red	mRFP1	584/607	(111)	(18)	Folds in the periplasm
	dTomato	554/581	(42)	(112)	Dimeric
II. New fluorescent proteins adapted for use in *B. burgdorferi:*					
Cyan	mCerulean	433/475	(37)	This study	A206K monomeric mutation
	msfCFP	NR[c]	(40)	This study	A206K mutation; superfolder
Green	mEGFP	489/509	(38)	This study	A206K mutation
	msfGFP	485/NR[c]	(40)	This study	A206K mutation; superfolder
Yellow	mCitrine	516/529	(39)	This study	A206K mutation
	msfYFP	NR[c]	(40)	This study	A206K mutation; superfolder
Red	mCherry	587/610	(42)	This study	
Infrared	iRFP	690/713	(43)	This study	Dimeric

[a] Maximum excitation (Ex) and emission (Em) wavelengths; [b]values assumed to be those for ECFP and EYFP, respectively (20); [c]NR, not reported: values were not reported in the original publication, or could not be exactly inferred from excitation and emission graphs.

897

898

Table 4. Summary of antibiotic resistance markers used in *B. burgdorferi*[a]

Resistance gene	Antibiotic	MIC[b] (µg/mL)	Notes	References
I. Widely used resistance markers				
aphI	Kanamycin	<25	Cross-resistance to neomycin, lividomycin, paromomycin, ribostamycin	(45, 67)
aadA	Streptomycin	7[c]	Expected cross-resistance to spectinomycin	(66)
aacC1	Gentamicin	<15.6		(67)
ermC	Erythromycin	0.005	Resistance level varies among strains; May pose safety risk	(68, 113, 114)
II. Newly developed resistance markers				
bsd^{Bb}	Blasticidin S	<5	Neither marker provides cross-resistance to the selection antibiotics listed above.	This study
hph^{Bb}	Hygromycin B	<200		This study

[a]For space considerations, this table does not contain a comprehensive list of antibiotic resistance markers developed for use in *B. burgdorferi*. For a detailed discussion of other markers, please see (13); [b]Minimal inhibitory concentration, determined in liquid culture; [c]Value is that of an inhibitory dose 50, or ID_{50}.

899

Figure 1

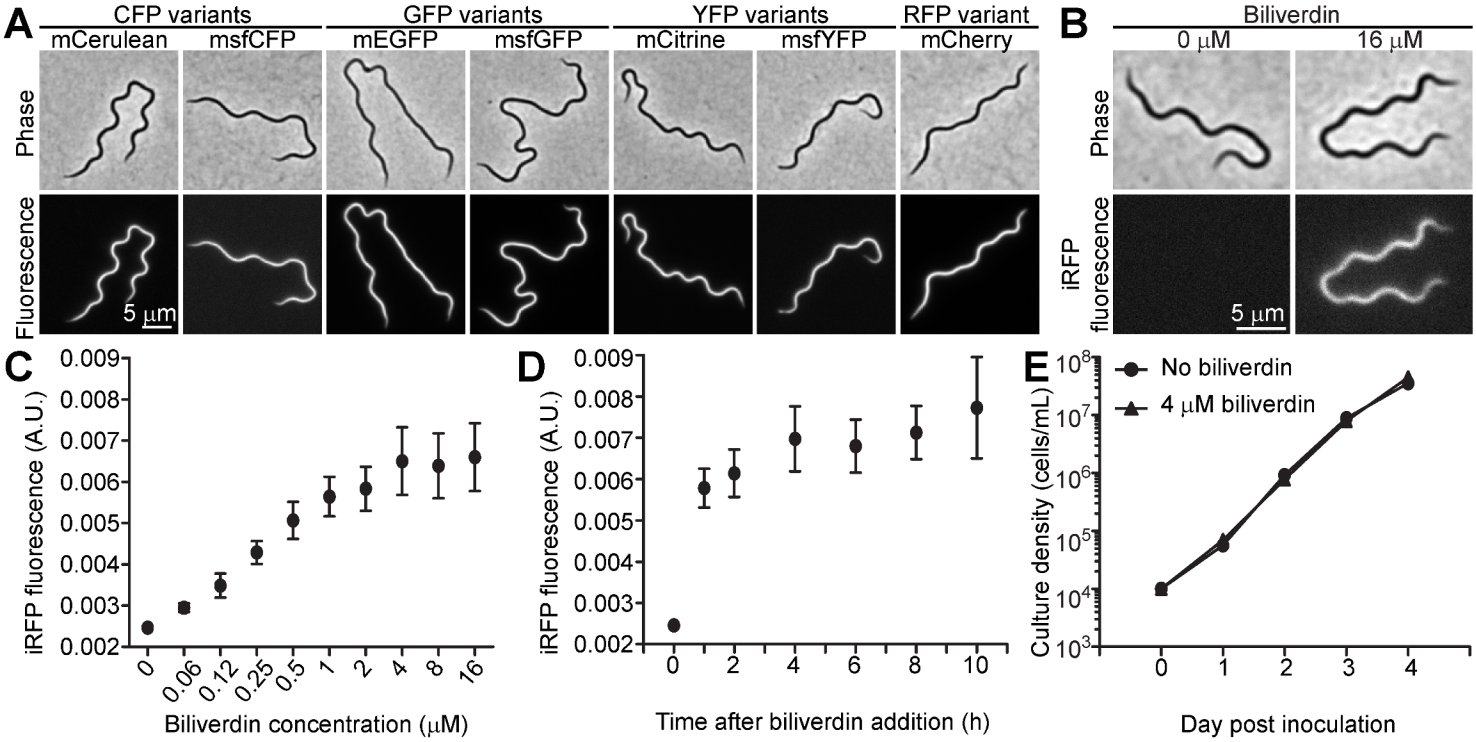

Figure 1. Fluorescent protein characterization. A. B. burgdorferi strains CJW_Bb090 through CJW_Bb096 expressing the indicated fluorescent proteins were imaged with matching filter sets. B. Strain CJW_Bb100 expressing iRFP requires biliverdin for development of fluorescence. Cells were grown in liquid culture with biliverdin for two days prior to imaging using a Cy5.5 filter set. C. Dose-response of iRFP fluorescence to biliverdin concentration. Strain CJW_Bb100 was grown in the presence of biliverdin for two days prior to imaging. Between 86 and 206 cells were analyzed for each concentration. Total cellular fluorescence levels were normalized by the cell area. Shown are means ± standard deviations (SD). A.U., arbitrary units. D. Time-course of iRFP fluorescence development in strain CJW_Bb100 following addition of 16 μM biliverdin. Between 68 and 110 cells were analyzed for each time point. E. Biliverdin does not affect B. burgdorferi growth. Strain CJW_Bb100 was inoculated at 104 cells/mL in duplicate in medium containing 4 μM biliverdin or no biliverdin, after which the spirochetes were enumerated daily.

Figure 2

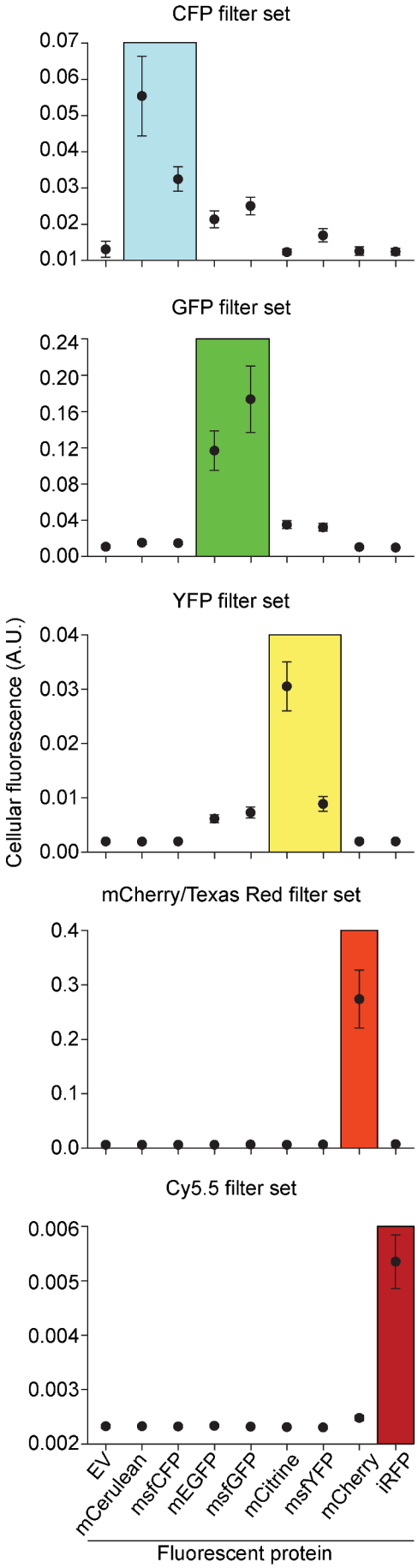

Figure 2. Quantification of fluorescent protein signal using common fluorescence filter sets. Strains CJW_Bb090 through CJW_Bb096 and CJW_Bb100 expressing the fluorescent proteins indicated at the bottom of the figure were each imaged using five filter sets: CFP, GFP, YFP, mCherry/TexasRed, and Cy5.5 (see the Materials and Methods section for filter set specifications). Strain CJW_Bb073 carrying an empty shuttle vector (EV) was also imaged to measure the cellular autofluorescence. Each filter set is listed at the top of the corresponding graph. Fluorescence intensity values were normalized by the cell area and are depicted as means ± SD in arbitrary units (A.U.). For each strain, 117 to 308 cells were analyzed. The iRFP strain was grown in the presence of 4 μM biliverdin for three days prior to imaging. The boxed region in each plot highlights the data obtained with filter sets that were ideal for the expressed fluorescent protein.

Figure 3

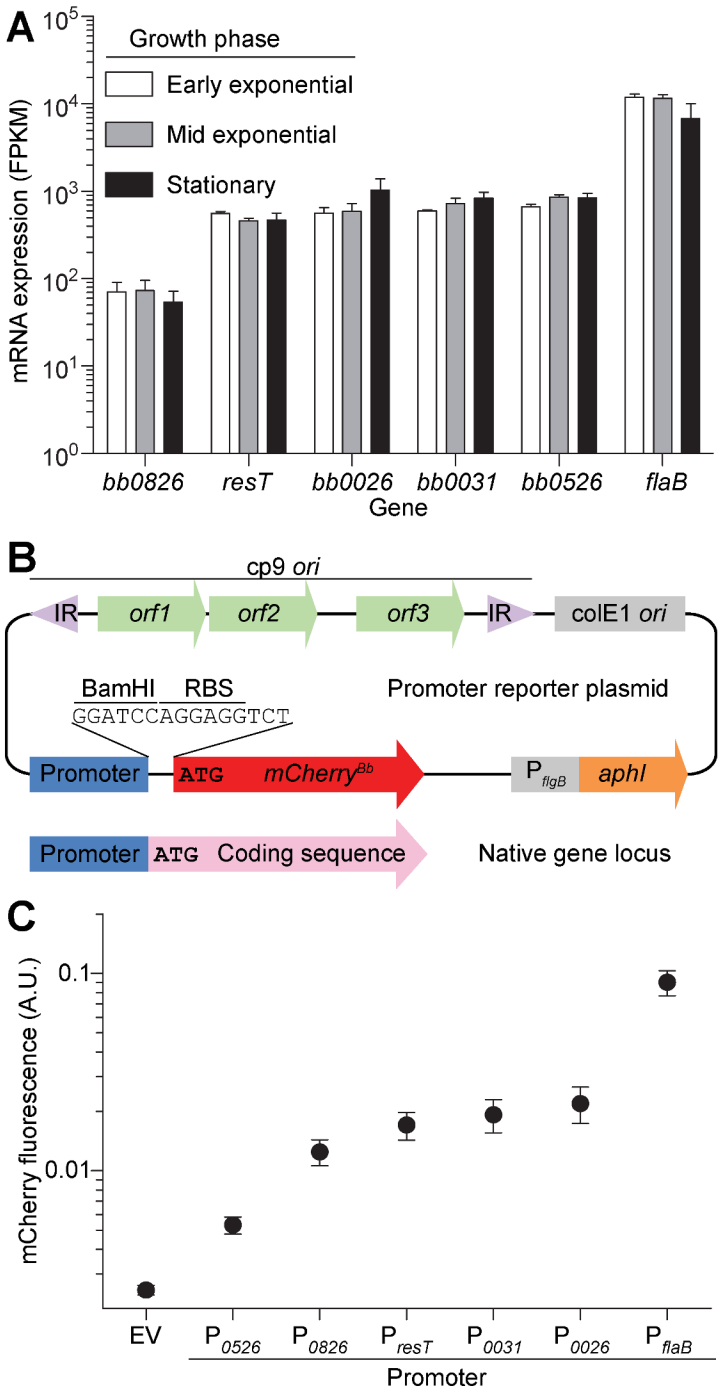

Figure 3. Promoter strength quantification. A. mRNA expression levels extracted from published RNA-seq data obtained using strain B31-A3 (99) grown to early exponential phase (10^6 cells/mL), mid-exponential phase (10^7 cells/mL), or stationary phase (one day after reaching 10^8 cells/mL) (64). FPKM, fragments per kilobase transcript per million mapped reads. B. Promoter reporter plasmid map (not drawn to scale). IR, inverted repeats; cp9 ori, origin of replication of B. burgdorferi plasmid cp9, which includes the genes orf1, orf2, orf3 needed for plasmid replication in B. burgdorferi; colE1 ori, E. coli origin of replication; P_{flgB}, B. burgdorferi flagellar rod operon promoter; aphI, kanamycin resistance gene. The promoter (blue) and the mCherry-coding sequence (red) are connected by a BamHI restriction enzyme site and a ribosomal binding site (RBS). The native locus from which the promoter was extracted is depicted below the plasmid map. The BamHI-RBS-mCherry sequence effectively replaced the native gene's protein coding sequence (shown in pink). Translational START sites are marked by the ATG codon. C. Promoter strength quantified by measuring cellular mCherry fluorescence in strains CJW_Bb069, CJW_Bb108 through CJW_Bb112, and CJW_Bb146. The fluorescence levels were normalized by cell area. The promoters were ranked in increasing order of the mean fluorescence values and are listed below the graph. Shown are means ± SD. Between 97 and 160 cells were analyzed per strain. EV, empty vector; A.U., arbitrary units.

Figure 4

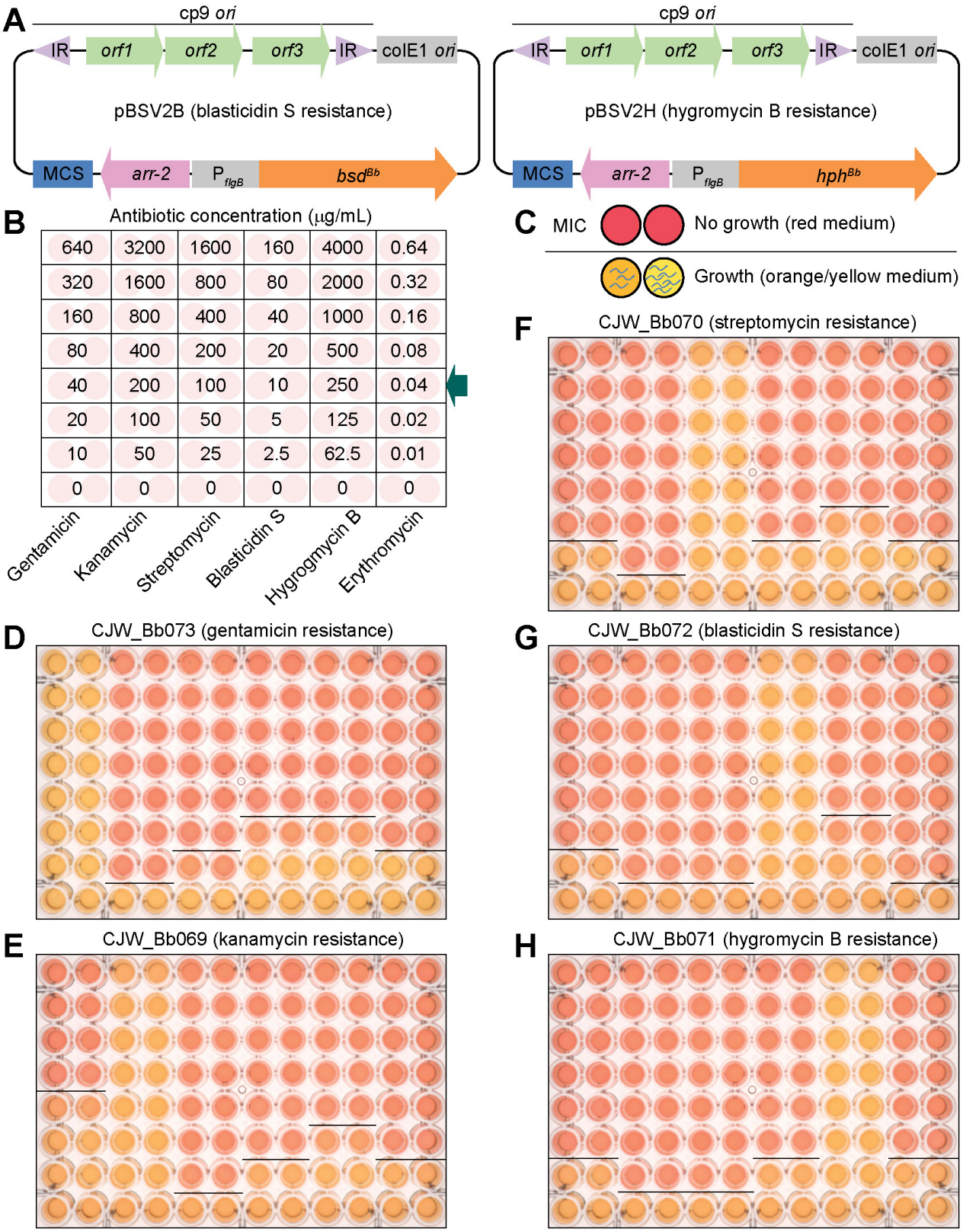

Figure 4. Characterization of blasticidin S and hygromycin B resistances in B. burgdorferi. A. Maps of shuttle vectors pBSV2B and pBSV2H. IR, inverted repeats; cp9 ori, origin or replication of B. burgdorferi plasmid cp9; colE1 ori, E. coli origin of replication; MCS, multicloning site; arr-2, rifampicin resistance gene for selection in E. coli; P_{flgB}, B. burgdorferi flagellar rod operon promoter; bsd^{Bb}, B. burgdorferi codon-optimized blasticidin S deaminase-encoding gene; hph^{Bb}, B. burgdorferi codon-optimized hygromycin B phosphotransferase-encoding gene. The maps are not drawn to scale. B. Plate map showing the final antibiotic concentrations used for cross-resistance testing. Each concentration was tested in two adjacent wells. Concentrations routinely used for selection are indicated by the arrow. C. Schematic representation of color change of the growth medium from red (absence of spirochete growth) to orange/yellow (presence of spirochete growth). A line marks the boundary between growth and no growth in an antibiotic concentration series. The lowest antibiotic concentration that blocked growth was identified as the minimal inhibitory concentration (MIC). D.-H. Susceptibility test of each resistance-carrying strain to various antibiotic concentrations according to the plate layout shown in B. The plates were incubated to allow for growth-dependent acidification of the medium and change in phenol red pH indicator color from red to orange and yellow, as depicted in panel C. Images were obtained using colorimetric imaging of the individual plates. MIC boundaries are marked by dark lines. The strains used are listed above each image.

Figure 5

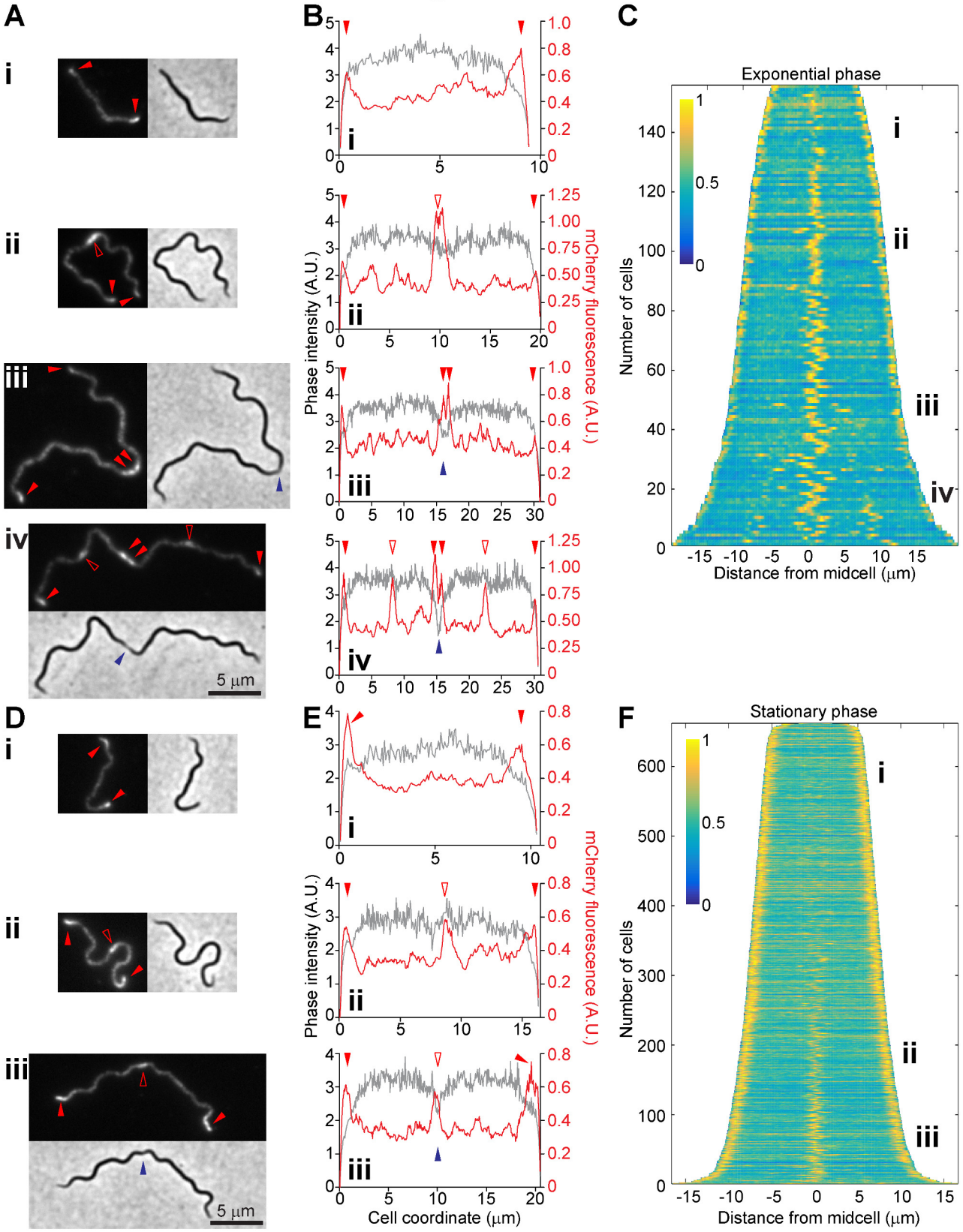

Figure 5. Localization of BB0323 using an mCherry fusion. A. Micrographs of cells of strain CJW_Bb173 imaged in exponential phase. Shown are mCherry fluorescence and phase contrast images. All images have the same magnification. Signal accumulation patterns are as follows: i, bipolar; ii, bipolar and midcell in the absence of obvious constriction in the phase contrast image; iii, bipolar and midcell in the presence of midcell constriction; and iv, bipolar, midcell in the presence of deep cell constriction, and at 1/4 and 3/4 positions along the cell length. B. Signal quantification along the cell length for cells shown in panel A. The mCherry signal is depicted in red, while the phase contrast signal is shown in gray. A and B. Polar localizations and midcell localizations flanking a deep constriction site are marked by filled red arrowheads. Midcell localizations are otherwise marked by empty red arrowheads. Indentation in the phase contrast signal is marked by blue arrowheads. C. Demograph depicting the localization of BB0323-mCherry in a population of exponentially growing cells of strain CJW_Bb173. See text for a detailed description. i-iv depict the regions on the demograph where cells with the localization patterns highlighted in panels A and B are located. D. Micrographs of cells of strain CJW_Bb173 imaged in stationary phase. Shown are mCherry fluorescence and phase contrast images. All images have the same magnification. Signal accumulation patterns are as follows: i, bipolar; ii, bipolar and midcell in the absence of cell constriction in the phase contrast image; and iii, bipolar and midcell in the presence of midcell constriction. E. Signal quantification as a function of cell length for cells shown in panel D. The mCherry signal is depicted in red, while the phase contrast signal is shown in gray. D and E. Filled and empty red arrowheads mark polar and midcell localization, respectively, whereas the blue arrowhead shows cell constriction. F. Demograph depicting the localization of BB0323-mCherry in a stationary phase population of cells of strain CJW_Bb173. i-iii depict the regions on the demograph where cells with the localization patterns highlighted in panels D and E are located.